A non-canonical function of Plk4 in centriolar satellite integrity and ciliogenesis through PCM1 phosphorylation

Akiko Hori[1, 2], Karin Barnouin[1], Ambrosius P. Snijders[1] and Takashi Toda[1, 3*]

[1]The Francis Crick Institute, Lincoln's Inn Fields Laboratory, 44 Lincoln's Inn Fields, London WC2A 3LY, United Kingdom.

[2]Developmental Biomedical Science, Graduate School of Biological Sciences, Nara Institute of Science and Technology (NAIST), 8916-5 Takayama, Ikoma, NARA 630-0192 Japan

[3]Hiroshima Research Center for Healthy Aging (HiHA), Department of Molecular Biotechnology, Graduate School of Advanced Sciences of Matter, Hiroshima University, 1-3-1 Kagamiyama, Higashi-Hiroshima, Japan 739-8530

[*]Correspondence should be addressed to Takashi Toda
Hiroshima Research Center for Healthy Aging (HiHA), Department of Molecular Biotechnology, Graduate School of Advanced Sciences of Matter, Hiroshima University, 1-3-1 Kagamiyama, Higashi-Hiroshima, Japan 739-8530
TEL: 81-082-424-7868
e-mail: takashi-toda@hiroshima-u.ac.jp

Keywords: centrosome; centriolar satellites; ciliogenesis; PCM1; Plk4; phosphorylation
Running Head: Linking Plk4 to centriolar satellites

Characters (excluding References and Materials and Methods): 24,159

Abstract

Centrioles are the major constituents of the animal centrosome, in which Plk4 kinase serves as a master regulator of the duplication cycle. Many eukaryotes also contain numerous peripheral particles known as centriolar satellites. While centriolar satellites aid centriole assembly and primary cilium formation, it is unknown whether Plk4 plays any regulatory roles in centriolar satellite integrity. Here we show that Plk4 is a critical determinant of centriolar satellite organisation. We found that Plk4 depletion led to the dispersion of centriolar satellites and perturbed ciliogenesis. Plk4 interacted with the

satellite component PCM1, and its kinase activity was required for phosphorylation of the conserved S372. The non-phosphorylatable mutant recapitulated Plk4 depletion, while the phospho-mimetic mutant rescued the dispersed patterns in cells depleted for either PCM1 or Plk4, albeit partially. We showed that S372 phosphorylation occurs during G1 and is important for PCM1 dimerisation and interaction with other satellite components. Our findings illuminate the requirement of Plk4 for centriolar satellite function, which may account for the underlying aetiology of ciliogenesis defects caused by Plk4 dysfunction.

Introduction

The centrosome consists of two orthogonally arranged centrioles that are surrounded by the pericentriolar material, and plays a multifaceted role in a wide range of biological processes as a major microtubule organising centre (MTOC) [1]. Importantly, in normal physiological conditions the centrosome cycle is under strict control regulated by both cell cycle and developmental cues [2]. Plk4 is a conserved protein kinase that executes a pivotal role in the centriole duplication cycle [3]. This kinase is critically a dose-dependent regulator; when malfunctioning the centrioles fail to duplicate, while when overproduced the centrioles undergo overamplification [4-8]. Plk4 is therefore unanimously regarded as a master kinase for centriole copy number control [3]. In support of this, it has recently been identified that mutations in *Plk4* lead to primordial dwarfism, and abnormal gene amplification results in human embryos exhibiting aneuploidy [9-11].

When starved of serum and/or treated under differentiation signals, cells exit the cell cycle and proceed into the ciliogenesis programme in many cell types [12-14]. Primary cilia are cellular antennas that serve to orchestrate key signalling events required for development. Over the past ten years, a number of genes encoding centriole/basal body components have been attributed as responsible for a group of human diseases collectively referred to as ciliopathies [13, 14]. Despite these advances, our knowledge of the regulatory mechanisms underlying primary cilium formation is far from comprehensive.

Aside from the core architecture of the centrosome, there has been much focus on pericentrosomal structures called the centriolar satellites [15, 16]. These non-membranous granules of 70-100 nm in size were originally found through the identification of PCM1 that localises around the centrosome as numerous foci [17, 18]. These particles move dynamically towards the centrosome, dependent upon microtubules and the dynein motor. The complete physiological roles of the centriolar satellites have not yet been elucidated; however at least one of the critical functions is the delivery of

centrosomal/ciliary components from the cytoplasm to the centrosome, which aids the formation of the centrosome and primary cilium [17, 19-26].

Although Plk4 is essential for centriole duplication, it has not been addressed whether this kinase plays any roles in centriolar satellite integrity. In this study we have investigated this proposition. We show that Plk4 is required for the spatial distribution and organisation of centriolar satellites separable from its role in centriole duplication. This role is executed by Plk4-dependent phosphorylation of PCM1.

Results and Discussion

Plk4 and its kinase activity are required for centriolar satellite integrity

In order to address whether the centrosome/centriole has any impact on centriolar satellite integrity, we first examined the emergence of centriolar satellites under conditions where Plk4 was depleted. Intriguingly, we found that Plk4 knockdown in U2OS cells led to the dispersal of centriolar satellite foci away from the vicinity of the centrosome (detected by an anti-PCM1 antibody) (Fig 1A-C). In line with a previous report [27], Plk4 knockdown resulted in reduced levels of hSAS-6, the procentriolar component essential for centriole duplication [28, 29]. However, unlike under Plk4 depletion, hSAS-6 depletion did not display the dispersion of PCM1 (Fig 1B and C). Notably, immunoblotting showed that the total protein levels of PCM1 were not significantly altered upon Plk4 depletion, though a modest reduction was seen (Fig 1A).

Consistent with the notion that PCM1 serves as a structural platform for centriolar satellite assembly [19, 30], other components including hMsd1/SSX2IP [23, 25, 26, 31] and BBS4 [32] were simultaneously dispersed upon Plk4 knockdown (Figs 1D, E, EV1A and B). On the contrary, silencing of Plk4 had no effect on the cytoplasmic localisation of dynein (Fig EV1C). The dispersal of PCM1 upon Plk4 knockdown was not specific to U2OS cells, as the same result was observed in Plk4-depleted HeLa cells (Fig EV1D-F).

In order to address whether satellite dispersion is induced independently of Plk4's role in centriole duplication, U2OS cells were first arrested in G1 phase, followed by Plk4 siRNA treatment (Fig EV1G-I). We found that under this condition, centriolar satellites also became scattered (Fig 1F and G). Hence, the role of Plk4 in centriolar satellite organisation is separable from that of centriole duplication. We then questioned whether Plk4 protein kinase activity was required. U2OS cells were first treated with Plk4-targeting siRNA, followed by ectopic introduction of RNAi-resistant myc-tagged wild type (WT*) or kinase-dead Plk4 (KD*). While Plk4-WT* effectively ameliorated the pericentrosomal localisation of PCM1, the introduction of Plk4-KD* was not able to rescue

the dispersion of PCM1 (Figs 1H, I, EV1J and K). Taken together, we conclude that Plk4 kinase activity plays a critical role in the pericentrosomal localisation of centriolar satellites.

PCM1 physically interacts with Plk4 and is phosphorylated at S372

To test whether PCM1 and Plk4 physically interact within cells, we performed immunoprecipitation. We found ectopically produced EGFP-PCM1 coimmunoprecipitated with endogenous Plk4 (Fig 2A) and exogenous myc-Plk4 bound endogenous PCM1 (Fig 2B). In contrast, immunoprecipitates with an anti-myc antibody (myc-Plk4) did not contain other PCM1-interacting proteins such as hMsd1/SSX2IP [23, 25, 26, 31] and BBS4 [32] (Fig 2A and B). Furthermore, bacterially produced and purified Plk4 and PCM1 also interacted in vitro (Fig. 2C). These results indicate that the interaction between Plk4 and PCM1 was direct. It is noteworthy that recent proteomics data also identified PCM1 as one of the Plk4-binding proteins [24] and furthermore, that the satellite component Mib1 ubiquitin ligase is involved in proteasome-mediated degradation of Plk4 [33].

We further asked whether PCM1 was phosphorylated and if Plk4 was able to bind phospho-PCM1. Total cell extracts were prepared from U2OS cells producing myc-tagged Plk4-WT* in which endogenous Plk4 was depleted, and immunoprecipitation was performed with an anti-myc antibody. Pulled-down beads were incubated in the presence or absence of λ-phosphatase and its inhibitors. λ-phosphatase treatment clearly indicated that PCM1 is a phosphoprotein (Fig EV2A). Collectively, the centriolar satellite component PCM1 is phosphorylated and interacts with Plk4.

Next, we implemented semi-quantitative liquid chromatography–mass spectrometry (LC-MS) to identify the phosphorylation sites within PCM1 that are dependent upon Plk4. Endogenous PCM1 was immunoprecipitated from HeLa cells that were treated with control or Plk4 siRNA. Precipitated PCM1 was cut out from gels (Fig EV2B) and analysed by LC-MS. Inspection of phosphopeptides identified five phospho-sites in the samples treated with control siRNA, of which only one site S372 was hypo-phosphorylated upon Plk4 knockdown (Fig EV2C-E). S372 is conserved within vertebrate PCM1 homologues and locates in the coiled coil rich N-terminal region, although S372 itself is not included within the coiled-coil domain (Fig 2D). It is of note that previous phosphoproteomic studies also identified S372 as one of the in vivo phosphorylation sites of PCM1 [34, 35].

We constructed EGFP-tagged PCM1 mutants containing non-phosphorylatable (S372A*) or phospho-mimetic versions (S372D* and S372E*) in an siRNA-resistant manner (*), and introduced them into cells in which endogenous PCM1 was depleted. Cells producing PCM1-S372A* or -S372E* contained the comparative levels of PCM1 to

WT*, and S372D* was somewhat underproduced (Fig EV2F). Interestingly, the mobility of PCM1-S372A* detected by either anti-GFP or anti-PCM antibodies was slightly faster than that of PCM-WT*, presumably reflecting the in vivo phosphorylation of PCM1 at this site (Fig EV2F).

We then prepared a phospho-specific antibody against S372. This antibody recognised phospho-S372 only in samples prepared by pull down (Fig EV2G). Accordingly, we performed immunoprecipitation from cells blocked at different cell cycle stages. As shown in Fig 2E, we found that S372 phosphorylation peaked during G1 phase. Therefore, Plk4 is responsible for PCM1 phosphorylation at S372.

PCM1 phosphorylation at S372 is critical for its pericentriolar localisation

We next examined the behaviour of PCM1 phospho-mutants within cells in which endogenous PCM1 was depleted. While wild type PCM1 localised to the pericentriolar region precisely as the endogenous proteins (see Fig 1B), PCM1-S372A* displayed dispersed patterns similar to wild type PCM1 proteins upon Plk4 depletion (Fig 3A and B). In stark contrast, PCM1-S372D* or PCM1-S372E* localised to the pericentriolar region, although notably in a more concentrated manner only around the centrosome (classified as “aggregated” in Fig 3B).

We further asked whether the phosphorylation of PCM1 at S372 is responsible for the dispersion of centriolar satellites upon Plk4 depletion. To this end, PCM1-WT*, -S372A*. -S372D* or -S372E* was introduced into U2OS cells depleted of Plk4. While neither PCM1-WT nor PCM1-S372A* was capable of rescuing the dispersed localisation of PCM1, ~50% of cells expressing PCM1-S372D* or PCM1-S372E* showed aggregated appearance in a similar manner to those seen in the presence of Plk4 (Fig3C and D). We also found that in addition to PCM1, other satellite components including hMsd1/SSX2IP, BBS4 and Cep290 [23, 25, 26, 31, 32, 36, 37], became dispersed in cells producing PCM1-S372A* (Fig EV3A-C). These results established that Plk4 is responsible for the pericentrosomal distribution of centriolar satellites mediated through phosphorylation of PCM1 at S372. Furthermore, reverse dephosphorylation is likely to be important for the dissolution of these particles.

S372 phosphorylation is important for dimerisation of PCM1 and its interaction with other satellite components

We investigated the mechanism by which PCM localisation is regulated through S372 phosphorylation. It is known that PCM1 forms oligomers, which lead to granular PCM1 in cells [19, 38]. Furthermore, S372 is situated within the region that is required for self-oligomerisation of PCM1 (201-494) [38] (see Fig 2D). We first asked whether S372

phosphorylation is essential for an intermolecular protein-protein interaction. For this purpose, we constructed plasmids producing differentially tagged PCM1 constructs (EGFP and mCherry) of WT* and S372A*, and transfected them in various combinations into cells in which endogenous PCM1 was depleted. Immunoprecipitation with an anti-RFP antibody (which recognises mCherry-PCM1) indicated that mCherry-PCM1-S372A* displayed reduced binding to EGFP-PCM1-WT* and EGFP-PCM1-327A* (Fig 3E). Furthermore, PCM1-S372A* showed compromised interaction with its binding partners such as BBS4 and Cep290, but not hMsd1/SSX2IP (Fig 3F). These results suggested that S372 phosphorylation plays a critical role in PCM1 dimerisation and interaction with other satellite components.

Next, we analysed the motility of PCM1-WT* and PCM1-372E* proteins within the cell. Kymograph analysis of individual PCM1 particles clearly indicated that while PCM1-WT* displayed dynamic motility, PCM1-S372E* exhibited very static trajectories instead (Fig EV3D), and both tracking velocity and length were substantially suppressed in this phospho-mimetic mutant (Fig EV3E-G). Furthermore, other satellite components such as hMsd1/SSX2IP, BBS4 and Cep290 also colocalised with aggregated PCM1-S372E foci (Fig EV3H). Thus, S372 phosphorylation within PCM1 promotes interaction with itself and other satellite components, leading to more aggregation around the centrosome accompanied with reduced motility.

Plk4-mediated S372 phosphorylation promotes ciliogenesis

It is known that centriolar satellites play a crucial role in primary cilium formation [15, 36, 37, 39]. We therefore investigated whether Plk4-mediated S372 phosphorylation of PCM1 contributes to ciliogenesis. Using human telomerase-immortalised retinal pigmented epithelial cell lines (hTERT-RPE-1), we first confirmed that upon depletion of Plk4 but not hSAS-6, PCM1 localised in a diffused manner as in U2OS and HeLa cells (Fig EV4A-C). Furthermore, depletion of PCM1 or Plk4 impeded efficient ciliogenesis under serum deprivation (Fig 4A and B) as previously reported [30, 37, 40].

We next examined S372 phosphorylation in serum-starved RPE-1 cells and found that it was phosphorylated (Fig EV4D). We then exogenously produced EGFP-PCM1-WT* or -S372E* in RPE-1 cells upon depletion of endogenous PCM1. EGFP-PCM1-WT* foci localised as numerous dots in the vicinity of the basal body similar to endogenous PCM1 [36, 37] and effectively rescued the ciliogenesis deficiency (Fig 4C and D). EGFP-PCM1-S372E* also rescued the defect, albeit less efficiently compared to wild type (~40 % vs ~65%, Fig 4D) and displayed more concentrated aggregates around the basal body (Fig 4C). Although phospho-mimetic PCM1 appeared capable of rescuing

ciliogenesis defects, it might need some reservations. For instance, it is possible that phospho-mimetic PCM1 might interact with residual wild type PCM1, leading to the formation of functional PCM1 dimers. In clear contrast, however, expression of PCM1-S372A* mutants failed to rescue the ciliogenesis defect and furthermore exhibited the diffused localisation patterns (Fig 4C and D). We also produced PCM1-S372E* upon double depletion of Plk4 and PCM1; under this condition, however, the rescue of ciliogenesis was not readily observed, suggesting that Plk4 may have additional functions in ciliogenesis beyond the phosphorylation of PCM1. In summary, we have uncovered that Plk4-mediated phosphorylation of PCM1 at S372 plays a critical role in primary cilium formation.

Impact of PCM1 phosphorylation on centriolar satellite integrity

Although it remains to be established whether or not PCM1 is a direct substrate of Plk4, it is firmly shown that S372 phosphorylation is dependent upon Plk4 kinase activity. We found that PCM1-S372A resulted in the dispersion of PCM1 away from the centrosome. We also showed that this non-phosphorylatable PCM1 could not efficiently form homo-dimers and displayed compromised binding to BBS4 and Cep290. These findings lead us to propose that S372 phosphorylation plays a critical role in dimer/oligomer formation of PCM1 and interaction with other satellite components, which are prerequisites for its role in centriolar satellite integrity (Fig 4E). At the moment, we could not distinguish whether these two events are independent processes, one process is dependent upon the other, or these are mutually interdependent. In contrast to PCM1-S372A, PCM1-S372D (and PCM1-S372E) formed larger, less motile aggregates around the centrosome. We consider that the dephosphorylation of S372 renders PCM1 particles more motile. It is possible that dephosphorylation is required for destabilising the interaction between PCM1 and the dynein complex [36]. Centriolar satellites are known to dissolve during mitosis and reassemble upon mitotic exit and the following G1 phase [18, 19, 30]. It is, therefore, tempting to speculate that this cell cycle-dependent reorganisation of centriolar satellites might be coupled with oscillatory Plk4 activity [41] through PCM1 phosphorylation.

The role of Plk4 in ciliogenesis

Our study and recent reports in zebrafish, mouse and humans [10, 40, 42] have shown that Plk4 plays a critical role in ciliogenesis. It is well established that only the mother centriole differentiates into the basal body to assemble the primary cilium [12-14]. If Plk4 is solely responsible for centriole duplication, then how does Plk4 dysfunction lead to cilia defects? Studies using small molecule inhibitors specific for Plk4 has attributed ciliogenesis defects to the complete loss of centrioles/centrosomes upon prolonged

passages of drug-containing cultures [42]. However, studies in zebrafish in which Plk4 was knocked down through morpholino indicated the loss of photoreceptors, which is a characteristic of defective cilia function, as being substantially more penetrant than the disappearance of centrioles (>90% vs. 25%) [10] and a very similar result was reported in an siRNA-mediated depletion of Plk4 in human cells [40]. Furthermore, human individuals who carry a homozygous mutation in the *Plk4* gene suffer from ciliopathy-related retinopathy, although patients-derived fibroblasts still contain the centrosome [10]. In line with these reports, we show that ciliogenesis defects were observed in RPE-1 cells upon Plk4 depletion while the basal body was still retained (Fig 4A and C). It therefore appears that the complete disappearance of the centrosome/centriole may not be an absolute prerequisite of ciliogenesis defects derived from Plk4 dysfunction.

Plk4 is generally thought to be inactive during G1, in which centriole duplication is not initiated while cells undergo ciliogenesis [13, 14, 41]. It is possible that the requirement of Plk4 for centriolar satellite integrity and ciliogenesis might manifest its temporal function independent of that in centriole duplication. It is, however, of note that recent reports suggest that Plk4 might play a role in centriole duplication during G1 prior to S phase [43, 44]. Given these preceding data and our current results, we propose that Plk4 potentiates ciliogenesis to some degree through PCM1 phosphorylation. This safeguards centriolar satellite integrity, and promotes delivery of ciliary components to the basal body (Fig 4E). Therefore, Plk4 dysfunction may induce anomalies in humans at least in part, through ciliogenesis failure attributable to centriolar satellite disorganisation.

Materials and methods

Cell cultures

Human cervical cancer HeLa cells and osteo-sarcoma U2OS cells were cultured in high-glucose DMEM (Invitrogen) supplemented with 10% fetal bovine serum. Immortalised human pigment epithelial cells hTERT-RPE-1 were cultured in DMEM/F12 (Invitrogen) supplemented with 10% fetal bovine serum and 1% non-essential amino acid. HeLa and U2OS cells were cultured in a humidified 5% CO2 incubator at 37℃ and hTERT-RPE-1 cells were cultured in a 10% CO2 incubator at 37℃. HeLa stably expressing GFP-centrin cells (kindly provided by Michel Bornens, Institut Curie, Paris, France) were cultured in DMEM supplemented with 10% fetal bovine serum and 0.5 mg/ml G418. For time-lapse imaging, cells were mounted in L15 media supplemented with 10% FBS.

RNA interference

Synthetic siRNA oligonucleotides were obtained from Dharmacon-GE Healthcare (Lafayette). The siRNA sequences were 5'-CUGGUAGUACUAGUUCACCUA-3' (Plk4 siRNA), 5'-GGCUUUAACUAAUUAUGGA-3' (PCM1 siRNA), or 5'-GCACGUUAAUCAGCUACAAUU -3' (hSAS-6 siRNA). Control depletion was carried out using siGENOME non-targeting siRNA (Dharmacon). For RNAi experiments, cells were transfected with 40 nM of dsRNA using Lipofectamine RNAi-MAX (Invitrogen), and cells were fixed 48 h after siRNA treatment unless otherwise stated.

Plasmid construction and DNA transfection

pEGFP-hPCM1 was a gift from Song-Hai Shi (Memorial Sloan Kettering Cancer Center, NY, USA). pcDNA-myc-Plk4 was a gift from Erich Nigg (Biozentrum, University of Basel, Switzerland). pmCherry-α-tubulin was obtained from Addgene. Plasmids containing various forms of PCM1 or Plk4 were constructed with appropriate PCR primer pairs. The amplified products were each subcloned into pEGFP-C1 and pmCherry-C1 (Clontech). pMBP-Plk4 (WT and KD) and p6His-PCM1 (containing amino acids 1-1128) were constructed in pMAL (New England BioLabs) and pETM-6His (a gift from Thomas Surrey) respectively. For construction of RNAi-resistant versions, we introduced 4 or 6 silent substitutions within the PCM1 or Plk4 siRNA-target region. The PCM1 siRNA target region, 5'- GGCTTTAACTAATTATGGA -3', was changed to 5'- AGCCCTGACTAATTATGGA -3' using site-directed mutagenesis with the primers, 5'-ctccacttccataattagtcagggcttgagtttcagctttagacaaattaatagacactggac-3' and 5-gtccagtgtctattaatttgtctaaagctgaaactcaagccctgactaattatggaagtggag -3'. The Plk4 siRNA target region, 5'- CTGGTAGTACTAGTTCACCTA -3', was changed to 5-CTGGCAGCACGAGCTCTCCAA -3' using site-directed mutagenesis with the primers, 5'-caataatcataggaagaaaacctggcagcacgagctctccaaaggccttatcacctcctccttctg -3' and 5-cagaaggaggaggtgataaggcctttggagagctcgtgctgccaggttttcttcctatgattattg -3'. RNA resistant constructs were denoted by an asterisk (*, i.e. Plk4-WT*). Plk4-KD* (K41R/D154A) was made by site-directed mutagenesis (QuikChange Lightning). Serine 372 within PCM1 was further mutated to alanine (S372A), aspartate (S372D) or glutamate (S372E).

Cells were treated with siRNAs for 48 h and observed under the microscope. For double transfection experiments, cells were treated with siRNAs for 48 h, followed by the second transfection with various plasmids. Cells were observed under the microscope 24 later.

Cell cycle synchronisation

For G1 cell cycle arrest, U2OS cells were doubly treated with Mimosine (0.2 mM; Sigma) for 16 h each prior to further siRNA treatment. Immunofluorescence microscopy and

immunoblotting were performed 24 h and 48 h later. For G2- and M-phase arrest, U2OS cells were treated for 24 h with RO-3306 (1 μM; ENZO Life Sciences) and Nocodazole (50 ng/ml; Sigma), respectively.

Recombinant protein expression and purification

Plasmids producing MBP, MBP-Plk4-WT or MBP-Plk4-KD were introduced into *E. coli* strain BL21-CodonPlus(DE3)-RIL (Agilent Technologies), and protein expression was induced by adding 0.05 mM IPTG at 18℃ for 16 h. Subsequently, proteins were purified on Amylose resin (New England Biolabs) according to manufacturer's instructions and concentrated by Vivaspin 20 (GE Healthcare). Purified proteins were stored in MBP buffer (20 mM Tris-HCl pH 7.5, 100 mM NaCl, 1 mM DTT, 10% Glycerol, EDTA-free complete protease inhibitor cocktail (Roche)). The recombinant His-PCM1(1128) protein was produced essentially in the same manner as above. Proteins were purified on complete His-Tag Purification resin (Roche) according to manufacturer's instructions. Fusion protein was eluted with elution buffer (20 mM Tris-HCl pH 7.5, 100 mM NaCl, 300 mM Imidazole, 1 mM DTT, 10% Glycerol, EDTA-free complete protease inhibitor cocktail). Eluted protein was desalted into a final buffer (20 mM Tris-HCl pH 7.5, 100 mM NaCl, 1 mM DTT, 10% Glycerol) using PD-10 Desalting columns (GE Healthcare) and concentrated by Vivaspin 20.

In vitro binding assay

For in vitro binding assay, MBP, MBP-Plk4-WT or MBP-Plk4-KD was mixed with Dynabeads Protein G (Invitrogen) coupled with an anti-MBP antibody. 8 μg of His-PCM1(1128) was treated with 600 μl binding buffer (50 mM Tris-HCl pH 7.5, 200 mM NaCl, 1 mM DTT, 2 mM MgCl2, 0.5 mg/ml BSA, 10% Glycerol, 0.05% NP-40, EDTA-free complete protease inhibitor cocktail) and incubated at 4℃ for 2 h. After several washes with the binding buffer (without BSA), beads were boiled in Laemmili sample buffer and applied to SDS-PAGE. Gels were stained with Coomassie Brilliant Blue or immunoblotted using antibodies against MBP, His or phospho-S372.

Antibodies

For immunofluorescence microscopy, the following antibodies were used: chicken anti-GFP (1:300, ab13970; Abcam), chicken anti-myc (1:300, A-21281; Molecular Probes-Thermo Fisher Scientific), rabbit anti-SSX2IP (1:150, HPA027306; Sigma-Aldrich), rabbit anti-PCM1 (1:300, sc67204; Santa Cruz Biotechnology), rabbit anti-γ-tubulin (1:250, T5192; Sigma-Aldrich), mouse anti-α-tubulin (1:250, T9026, Sigma-Aldrich), mouse anti-Plk4 (1:200, H00010733-B01; Abnova), mouse anti-Glu-tubulin (1:150, AB3201; Merck Millipore), anti-DIC (1:150, MAB1618; Merck Millipore), anti-BBS4 (1:100, Abnova), anti-

MBP (1:10000, New England Biolabs) and anti-His antibodies (1:2000, Novagen). Secondary antibodies were Alexa Fluor 488-coupled anti-rabbit, Alexa Fluor 594-coupled anti-rabbit, Alexa Fluor 594-coupled anti-mouse, Alexa Fluor 488-coupled anti-mouse, Alexa Fluor 488-coupled anti-chicken, or Cy3-coupled anti-mouse antibodies (all used at 1:1,500, Molecular Probes). For immunoblotting, the following antibodies were used: mouse anti-GFP (1:1,000, 11814460001; Roche), mouse anti-Cherry (1:1,000, 632543; Clontech), mouse anti-myc (1:1,000, MMS-150R; Babco), rabbit anti-hSAS-6 (1:1000, sc98506; Santa Cruz Biotechnology), rabbit anti-PCM1 (1:2,000), mouse anti-Plk4 (1:1,000), rabbit anti-SSX2IP (1:1,000), anti-DIC (1:1,000), anti-BBS4 (1:1,000), rabbit anti-γ-tubulin and mouse anti-α-tubulin antibodies (1:5,000).

Rabbit polyclonal phospho-specific antibody raised against phospho-peptide (CQAESLS^{PO3H2}LTREVS) was generated and affinity-purified by Eurogentec. This antibody recognises phospho-S372 only when PCM1 is pulled down from whole cell extracts; we could not detect phosphorylated PCM1 with simple immunoblotting against total protein lysates or immunofluorescence microscopy.

LC-MS analysis

1.5 mg of total protein extracts were prepared from HeLa cell cultures treated with control or Plk4 siRNA, and immunoprecipitation performed with an anti-PCM1 antibody. Colloidal coomassie-stained bands corresponding to precipitated PCM1 were cut out from gels and subject to trypsin digestion [45] and Q Exactive LC-MS analysis (Thermo Fisher Scientific). The data was searched against human Uniprot (UniProt KB2012_08 taxonomy human 9606 canonical with contaminants 20120921) using the Andromeda search engine and MaxQuant (Version 1.3.0.5) [46], as well as Mascot Daemon search engines (version 2.4.0, Matrix Science). For MaxQuant, a false discovery rate of 0.1% was used to generate protein and peptide identification tables. The data was uploaded into Perseus (MaxQuant) for further statistical analyses. Skyline software was employed for label-free quantification (version 3.1) [47]. The extracted ion chromatograms were manually curated to ensure accurate peak-picking and quantification.

Immunofluorescence microscopy and image analysis

Immunofluorescence microscopy was performed as described previously [25, 26]. Briefly, cells were fixed with methanol at −20°C for 5 min and washed in PBS. After blocking in 3% BSA for 1 h at room temperature, cells were incubated with primary and then secondary antibodies. DNA was visualised by the addition of DAPI (4,6-diamidino-2-phenylindole; Vector Lab). During time-lapse imaging, cells were kept at 34-37℃ by a chamber heater.

Images were taken using an Olympus IX71 wide-field inverted epifluorescence microscope with Olympus PlanApo 60×, NA 1.4, or UApo 40×, NA 1.35, oil immersion objectives (Olympus). DeltaVision image acquisition software (softWoRx 3.3.0; Applied Precision Co.) equipped with Coolsnap-HQ digital CCD camera or Cascade EMCCD 512B camera (Roper Scientific) was used. The sections of images were compressed into a two-dimensional (2D) projection using the DeltaVision maximum intensity algorithm. Deconvolution was applied before generating the 2D projection. Images were taken as 64 sections along the z-axis at 0.2 μm intervals. Captured images were processed with Adobe Photoshop CS3 (version 10.0).

The localisation patterns of centriolar satellite components were categorised by visual inspection. When multiple immunofluorescence signals of satellite components were found at the centrosome region (marked by anti-γ-tubulin dots), they were categorised as "normal". In contrast, when these signals were dispersed away from the centrosome, they were classified as "dispersed". When signals formed larger aggregates, they were scored as "aggregated".

Immunoprecipitation

For coimmunoprecipitation, 1 mg cell lysate was incubated with 30 μl GFP-Trap or RFP-Trap (ChromoTek) in lysis buffer (25 mM Tris-HCl, pH 7.0, 1 mM EDTA, 300 mM NaCl, 10% Glycerol, 1% NP-40, 1 mM DTT, 10 mM NaF, 25 mM DMSF and EDTA-free protease inhibitor tablet (Complete: Roche) overnight at 4 ℃. After washing with lysis buffer, the beads were denatured at 95 ℃ in NuPAGE buffer (Invitrogen) and run on SDS-PAGE, followed by immunoblotting.

Quantification and fluorescence signal intensity measurement

For fluorescence signal intensity measurement, fluorescence signals were quantified using maximum intensity, after subtracting background signals in the vicinity of the fluorescent spot. The SoftWoRx software was used for analysis. At least 200 cells were counted in each sample, independently, three times, from which standard deviations and P-values were calculated.

Tracking the trajectory of PCM1 motility

U2OS cells were treated with PCM1 siRNA for 48 h and then further transfected with pmCherry-α-tubulin and pEGFP-PCM1-WT* or pEGFP-PCM1-S372E* plasmids. 18 h after the second transfection, live imaging was started. Movie streams were acquired at a frame rate of 2 frame/s. Subsequent particle tracking analysis was carried out using Imaris software (Bitplane). Briefly, the diffusion trajectories of single particles were determined by connecting the spots corresponding to individual time points.

Statistical data analysis

All data represent the mean of multiple experiments +/- SD. Experiment sample numbers and the number of replicates used for statistical testing have been reported in the corresponding figure legends. All p-values are from two-tailed unpaired student t-tests. Unless otherwise stated, we followed this key for asterisk placeholders for p-values in the figures: ****p<0.0001, ***p<0.001, **p<0.01, *p<0.05.

Expanded View Figures

Expanded View Figures (EV1-4) and legends can be found on line.

Acknowledgments

We thank Michel Bornens, Erich Nigg, Wei Shao, Song-Hai Shi and Thomas Surrey for reagents. We thank Yasuto Murayama for reagents and technical advice. We are grateful to Risa Mori for critical reading of the manuscript. T.T. and A.P.S were supported by Cancer Research UK.

Author contribution

The experiments were designed by A.H. and T.T., A.H. performed the majority of the experiments and data analysis, and K.B. performed LC-MS and together with A.P.B. conducted comparative analysis of phosphopeptides. A.H. and T.T. wrote the paper with suggestions from K.B. and A.P.S.

Conflict of Interest

The authors declare no conflict of interest arising from this work.

References

1. Luders, J. & Stearns, T. (2007) Microtubule-organizing centres: a re-evaluation, *Nat Rev Mol Cell Biol.* **8**, 161-167.

2. Fu, J., Hagan, I. M. & Glover, D. M. (2015) The centrosome and Its duplication cycle, *Cold Spring Harb Perspect Biol.* **7**, a015800.

3. Nigg, E. A. & Stearns, T. (2011) The centrosome cycle: Centriole biogenesis, duplication and inherent asymmetries, *Nat Cell Biol.* **13**, 1154-1160.

4. Bettencourt-Dias, M., Rodrigues-Martins, A., Carpenter, L., Riparbelli, M., Lehmann, L., Gatt, M. K., Carmo, N., Balloux, F., Callaini, G. & Glover, D. M. (2005) SAK/PLK4 is required for centriole dplication and flagella development, *Curr Biol.* **15**, 2199-2207.

5. Kleylein-Sohn, J., Westendorf, J., Le Clech, M., Habedanck, R., Stierhof, Y. D. & Nigg, E. A. (2007) Plk4-induced centriole biogenesis in human cells, *Dev Cell.* **13**, 190-202.
6. Habedanck, R., Stierhof, Y. D., Wilkinson, C. J. & Nigg, E. A. (2005) The Polo kinase Plk4 functions in centriole duplication, *Nat Cell Biol.* **7**, 1140-1145.
7. O'Connell, K. F., Caron, C., Kopish, K. R., Hurd, D. D., Kemphues, K. J., Li, Y. & White, J. G. (2001) The *C. elegans zyg-1* gene encodes a regulator of centrosome duplication with distinct maternal and paternal roles in the embryo, *Cell.* **105**, 547-558.
8. Peel, N., Stevens, N. R., Basto, R. & Raff, J. W. (2007) Overexpressing centriole-replication proteins in vivo induces centriole overduplication and de novo formation, *Curr Biol.* **17**, 834-843.
9. McCoy, R. C., Demko, Z., Ryan, A., Banjevic, M., Hill, M., Sigurjonsson, S., Rabinowitz, M., Fraser, H. B. & Petrov, D. A. (2015) Common variants spanning PLK4 are associated with mitotic-origin aneuploidy in human embryos, *Science.* **348**, 235-238.
10. Martin, C. A., Ahmad, I., Klingseisen, A., Hussain, M. S., Bicknell, L. S., Leitch, A., Nurnberg, G., Toliat, M. R., Murray, J. E., Hunt, D., Khan, F., Ali, Z., Tinschert, S., Ding, J., Keith, C., Harley, M. E., Heyn, P., Muller, R., Hoffmann, I., Daire, V. C., Dollfus, H., Dupuis, L., Bashamboo, A., McElreavey, K., Kariminejad, A., Mendoza-Londono, R., Moore, A. T., Saggar, A., Schlechter, C., Weleber, R., Thiele, H., Altmuller, J., Hohne, W., Hurles, M. E., Noegel, A. A., Baig, S. M., Nurnberg, P. & Jackson, A. P. (2014) Mutations in PLK4, encoding a master regulator of centriole biogenesis, cause microcephaly, growth failure and retinopathy, *Nat Genet.* **46**, 1283-1292.
11. Shaheen, R., Al Tala, S., Almoisheer, A. & Alkuraya, F. S. (2014) Mutation in *PLK4*, encoding a master regulator of centriole formation, defines a novel locus for primordial dwarfism, *J Med Genet.* **51**, 814-816.
12. Kobayashi, T. & Dynlacht, B. D. (2011) Regulating the transition from centriole to basal body, *J Cell Biol.* **193**, 435-444.
13. Goetz, S. C. & Anderson, K. V. (2010) The primary cilium: a signalling centre during vertebrate development, *Nat Rev Genet.* **11**, 331-344.
14. Gerdes, J. M., Davis, E. E. & Katsanis, N. (2009) The vertebrate primary cilium in development, homeostasis, and disease, *Cell.* **137**, 32-45.
15. Barenz, F., Mayilo, D. & Gruss, O. J. (2011) Centriolar satellites: Busy orbits around the centrosome, *Eur J Cell Biol.* **90**, 983-989.
16. Tollenaere, M. A., Mailand, N. & Bekker-Jensen, S. (2014) Centriolar satellites: key mediators of centrosome functions, *Cell Mol Life Sci.* **72**, 11-23.

17. Kubo, A., Sasaki, H., Yuba-Kubo, A., Tsukita, S. & Shiina, N. (1999) Centriolar satellites: molecular characterization, ATP-dependent movement toward centrioles and possible involvement in ciliogenesis, *J Cell Biol.* **147**, 969-980.

18. Balczon, R., Bao, L. & Zimmer, W. E. (1994) PCM-1, A 228-kD centrosome autoantigen with a distinct cell cycle distribution, *J Cell Biol.* **124**, 783-793.

19. Dammermann, A. & Merdes, A. (2002) Assembly of centrosomal proteins and microtubule organization depends on PCM-1, *J Cell Biol.* **159**, 255-266.

20. Oshimori, N., Li, X., Ohsugi, M. & Yamamoto, T. (2009) Cep72 regulates the localization of key centrosomal proteins and proper bipolar spindle formation, *EMBO J.* **28**, 2066-2076.

21. Kim, K. & Rhee, K. (2011) The pericentriolar satellite protein CEP90 is crucial for integrity of the mitotic spindle pole, *J Cell Sci.* **124**, 338-347.

22. Staples, C. J., Myers, K. N., Beveridge, R. D., Patil, A. A., Lee, A. J., Swanton, C., Howell, M., Boulton, S. J. & Collis, S. J. (2012) The centriolar satellite protein Cep131 is important for genome stability, *J Cell Sci.* **125**, 4770-4779.

23. Barenz, F., Inoue, D., Yokoyama, H., Tegha-Dunghu, J., Freiss, S., Draeger, S., Mayilo, D., Cado, I., Merker, S., Klinger, M., Hoeckendorf, B., Pilz, S., Hupfeld, K., Steinbeisser, H., Lorenz, H., Ruppert, T., Wittbrodt, J. & Gruss, O. J. (2013) The centriolar satellite protein SSX2IP promotes centrosome maturation, *J Cell Biol.* **202**, 81-95.

24. Firat-Karalar, E. N., Rauniyar, N., Yates, J. R., 3rd & Stearns, T. (2014) Proximity interactions among centrosome components identify regulators of centriole duplication, *Curr Biol.* **24**, 664–670.

25. Hori, A., Peddie, C. J., Collinson, L. M. & Toda, T. (2015) Centriolar satellite- and hMsd1/SSX2IP-dependent microtubule anchoring is critical for centriole assembly, *Mol Biol Cell.* **26**, 2005-2019.

26. Hori, A., Ikebe, C., Tada, M. & Toda, T. (2014) Msd1/SSX2IP-dependent microtubule anchorage ensures spindle orientation and primary cilia formation, *EMBO Rep.* **15**, 175–184.

27. Puklowski, A., Homsi, Y., Keller, D., May, M., Chauhan, S., Kossatz, U., Grunwald, V., Kubicka, S., Pich, A., Manns, M. P., Hoffmann, I., Gonczy, P. & Malek, N. P. (2011) The SCF-Fbxw5 E3-ubiquitin ligase is regulated by Plk4 and targets HsSAS-6 to control centrosome duplication, *Nat Cell Biol.* **13**, 1004-1009.

28. Strnad, P., Leidel, S., Vinogradova, T., Euteneuer, U., Khodjakov, A. & Gonczy, P. (2007) Regulated HsSAS-6 levels ensure formation of a single procentriole per centriole during the centrosome duplication cycle, *Dev Cell.* **13**, 203-213.

29. Leidel, S., Delattre, M., Cerutti, L., Baumer, K. & Gonczy, P. (2005) SAS-6 defines a protein family required for centrosome duplication in *C. elegans* and in human cells, *Nat Cell Biol.* **7**, 115-125.

30. Lopes, C. A., Prosser, S. L., Romio, L., Hirst, R. A., O'Callaghan, C., Woolf, A. S. & Fry, A. M. (2011) Centriolar satellites are assembly points for proteins implicated in human ciliopathies, including oral-facial-digital syndrome 1, *J Cell Sci.* **124**, 600-612.

31. Hori, A., Morand, A., Ikebe, C., Frith, D., Snijders, A. P. & Toda, T. (2015) The conserved Wdr8-hMsd1/SSX2IP complex localises to the centrosome and ensures proper spindle length and orientation, *Biochem Biophys Res Commun.* **468**, 39-45.

32. Kim, J. C., Badano, J. L., Sibold, S., Esmail, M. A., Hill, J., Hoskins, B. E., Leitch, C. C., Venner, K., Ansley, S. J., Ross, A. J., Leroux, M. R., Katsanis, N. & Beales, P. L. (2004) The Bardet-Biedl protein BBS4 targets cargo to the pericentriolar region and is required for microtubule anchoring and cell cycle progression, *Nat Genet.* **36**, 462-470.

33. Cajanek, L., Glatter, T. & Nigg, E. A. (2015) The E3 ubiquitin ligase Mib1 regulates Plk4 and centriole biogenesis, *J Cell Sci.* **128**, 1674-1682.

34. Wang, B., Malik, R., Nigg, E. A. & Korner, R. (2008) Evaluation of the low-specificity protease elastase for large-scale phosphoproteome analysis, *Anal Chem.* **80**, 9526-9533.

35. Van Hoof, D., Munoz, J., Braam, S. R., Pinkse, M. W., Linding, R., Heck, A. J., Mummery, C. L. & Krijgsveld, J. (2009) Phosphorylation dynamics during early differentiation of human embryonic stem cells, *Cell stem cell.* **5**, 214-226.

36. Kim, J., Krishnaswami, S. R. & Gleeson, J. G. (2008) CEP290 interacts with the centriolar satellite component PCM-1 and is required for Rab8 localization to the primary cilium, *Hum Mol Genet.* **17**, 3796-3805.

37. Stowe, T. R., Wilkinson, C. J., Iqbal, A. & Stearns, T. (2012) The centriolar satellite proteins Cep72 and Cep290 interact and are required for recruitment of BBS proteins to the cilium, *Mol Biol Cell.* **17**, 3322-3335.

38. Kubo, A. & Tsukita, S. (2003) Non-membranous granular organelle consisting of PCM-1: subcellular distribution and cell-cycle-dependent assembly/disassembly, *J Cell Sci.* **116**, 919-928.

39. Nachury, M. V., Loktev, A. V., Zhang, Q., Westlake, C. J., Peranen, J., Merdes, A., Slusarski, D. C., Scheller, R. H., Bazan, J. F., Sheffield, V. C. & Jackson, P. K. (2007) A

core complex of BBS proteins cooperates with the GTPase Rab8 to promote ciliary membrane biogenesis, *Cell.* **129**, 1201-1213.

40. Wheway, G., Schmidts, M., Mans, D. A., Szymanska, K., Nguyen, T. M., Racher, H., Phelps, I. G., Toedt, G., Kennedy, J., Wunderlich, K. A., Sorusch, N., Abdelhamed, Z. A., Natarajan, S., Herridge, W., van Reeuwijk, J., Horn, N., Boldt, K., Parry, D. A., Letteboer, S. J., Roosing, S., Adams, M., Bell, S. M., Bond, J., Higgins, J., Morrison, E. E., Tomlinson, D. C., Slaats, G. G., van Dam, T. J., Huang, L., Kessler, K., Giessl, A., Logan, C. V., Boyle, E. A., Shendure, J., Anazi, S., Aldahmesh, M., Al Hazzaa, S., Hegele, R. A., Ober, C., Frosk, P., Mhanni, A. A., Chodirker, B. N., Chudley, A. E., Lamont, R., Bernier, F. P., Beaulieu, C. L., Gordon, P., Pon, R. T., Donahue, C., Barkovich, A. J., Wolf, L., Toomes, C., Thiel, C. T., Boycott, K. M., McKibbin, M., Inglehearn, C. F., Consortium, U. K., University of Washington Center for Mendelian, G., Stewart, F., Omran, H., Huynen, M. A., Sergouniotis, P. I., Alkuraya, F. S., Parboosingh, J. S., Innes, A. M., Willoughby, C. E., Giles, R. H., Webster, A. R., Ueffing, M., Blacque, O., Gleeson, J. G., Wolfrum, U., Beales, P. L., Gibson, T., Doherty, D., Mitchison, H. M., Roepman, R. & Johnson, C. A. (2015) An siRNA-based functional genomics screen for the identification of regulators of ciliogenesis and ciliopathy genes, *Nat Cell Biol.* **17**, 1074-1087.

41. Sillibourne, J. E. & Bornens, M. (2010) Polo-like kinase 4: the odd one out of the family, *Cell Div.* **5**, 25.

42. Wong, Y. L., Anzola, J. V., Davis, R. L., Yoon, M., Motamedi, A., Kroll, A., Seo, C. P., Hsia, J. E., Kim, S. K., Mitchell, J. W., Mitchell, B. J., Desai, A., Gahman, T. C., Shiau, A. K. & Oegema, K. (2015) Reversible centriole depletion with an inhibitor of Polo-like kinase 4, *Science.* **348**, 1155-1160.

43. Ohta, M., Ashikawa, T., Nozaki, Y., Kozuka-Hata, H., Goto, H., Inagaki, M., Oyama, M. & Kitagawa, D. (2014) Direct interaction of Plk4 with STIL ensures formation of a single procentriole per parental centriole, *Nat Commun.* **5**, 5267.

44. Fong, C. S., Kim, M., Yang, T. T., Liao, J. C. & Tsou, M. F. (2014) SAS-6 assembly templated by the lumen of cartwheel-less centrioles precedes centriole duplication, *Dev Cell.* **30**, 238–245.

45. Plaza-Menacho, I., Barnouin, K., Goodman, K., Martinez-Torres, R. J., Borg, A., Murray-Rust, J., Mouilleron, S., Knowles, P. & McDonald, N. Q. (2014) Oncogenic RET kinase domain mutations perturb the autophosphorylation trajectory by enhancing substrate presentation in trans, *Mol Cell.* **53**, 738-751.

46. Cox, J. & Mann, M. (2008) MaxQuant enables high peptide identification rates, individualized p.p.b.-range mass accuracies and proteome-wide protein quantification, *Nature Biotechnology.* **26**, 1367-1372.

47. Schilling, B., Rardin, M. J., MacLean, B. X., Zawadzka, A. M., Frewen, B. E., Cusack, M. P., Sorensen, D. J., Bereman, M. S., Jing, E., Wu, C. C., Verdin, E., Kahn, C. R., Maccoss, M. J. & Gibson, B. W. (2012) Platform-independent and label-free quantitation of proteomic data using MS1 extracted ion chromatograms in skyline: application to protein acetylation and phosphorylation, *Mol Cell Proteomics.* **11**, 202-214.

48. Dzhindzhev, N. S., Tzolovsky, G., Lipinszki, Z., Schneider, S., Lattao, R., Fu, J., Debski, J., Dadlez, M. & Glover, D. M. (2014) Plk4 phosphorylates Ana2 to trigger Sas6 recruitment and procentriole formation, *Curr Biol.* **24**, 2526–2532.

49. Kodani, A., Yu, T. W., Johnson, J. R., Jayaraman, D., Johnson, T. L., Al-Gazali, L., Sztriha, L., Partlow, J. N., Kim, H., Krup, A. L., Dammermann, A., Krogan, N. J., Walsh, C. A. & Reiter, J. F. (2015) Centriolar satellites assemble centrosomal microcephaly proteins to recruit CDK2 and promote centriole duplication, *eLife.* **4**, e07519.

50. Klinger, M., Wang, W., Kuhns, S., Barenz, F., Drager-Meurer, S., Pereira, G. & Gruss, O. J. (2014) The novel centriolar satellite protein SSX2IP targets Cep290 to the ciliary transition zone, *Mol Biol Cell.* **25**, 495-507.

51. Villumsen, B. H., Danielsen, J. R., Povlsen, L., Sylvestersen, K. B., Merdes, A., Beli, P., Yang, Y. G., Choudhary, C., Nielsen, M. L., Mailand, N. & Bekker-Jensen, S. (2013) A new cellular stress response that triggers centriolar satellite reorganization and ciliogenesis, *EMBO J.* **32**, 3029 - 3040.

Figure legends

Figure 1. Plk4 kinase activity is required for the pericentriolar distribution of centriolar satellite components

A. Evaluation of siRNA-mediated depletion. U2OS cells were treated with control, Plk4 or hSAS-6 siRNA and immunoblotting was performed with the indicated antibodies. Asterisk indicates non-specific bands. The positions of molecular weight markers (kDa) are shown on the right.

B. U2OS cells were transfected with the indicated siRNAs. Cell peripheries are marked with dotted lines. Enlarged single cell images (marked with arrowheads in the top row) are shown at the bottom. Scale bars, 5 μm (bottom),10 μm (top).

C, D, E. Quantification of the dispersion of satellite components upon depletion of Plk4 but not hSAS-6 knockdown. The results of PCM1 (**C**), hMsd1/SSX2IP (**D**) or BBS4 (**E**) are shown. Data represent the mean + SD (>200 cells, n=3). Statistical analysis was performed using two-tailed unpaired student's *t*-tests. **p<0.01, n.s. (not significant).

F, G. U2OS cells were arrested in G1 and treated with control or Plk4 siRNA, followed by immunofluorescence microscopy by using indicated antibodies. Enlarged images (marked by arrowheads) are shown on the right. Quantification of PCM1 distribution is shown in **G**. >200 cells were counted and classified into two categories: normal (around and away from the centrosome) or dispersed. Data represent the mean + SD (n=3). Statistical analysis was performed using two-tailed unpaired student's *t*-tests. **p<0.01. Scale bar, 1 μm (**F**, right), 10 μm (**F**).

H, I. siRNA-treated U2OS cells were transfected with empty vectors (EV) or plasmids containing Plk4 or siRNA-resistant Plk4-myc WT* or KD* and immunostained with the indicated antibodies. Cell peripheries are marked with solid lines, in which cells with yellow lines are successfully transfected (positive in myc signals), while those with white lines represent non-transfected cells. Quantification of PCM1 distribution is shown in **I**. Data represent the mean + SD (>200 cells, n=3). Statistical analysis was performed using two-tailed unpaired student's *t*-tests. ****p<0.0001, **p<0.01, n.s. (not significant). Scale bar, 5 μm (**H**).

Figure 2. PCM1 physically interacts with Plk4 and is phosphorylated at S372

A, B. Either empty vector plasmids (EV) or those producing EGFP-PCM1 (**A**) or myc-Plk4 (**B**) were transfected into U2OS cells. Immunoprecipitation (IP) was performed with anti-GFP (**A**) or anti-myc antibodies (**B**), followed by immunoblotting with the indicated antibodies. DIC, the dynein intermediate chain.

C. Bacterially expressed and purified His-PCM1 (a.a. 1-1128) was incubated with MBP alone or MBP-Plk4 (WT or KD) in vitro, and pulled down by magnetic beads coupled with an anti-MBP antibody, followed by staining with Coomassie Blue (left) or immunoblotting with an anti-His antibody (right). Asterisks show non-specific bands. The mobility difference between Plk4-WT and Plk4-KD was reported previously [43, 48]. We reproducibly observed the upward mobility shift of His-PCM1 upon binding to MBP-Plk4-WT, but not Plk4-KD.

D. Overall structure of PCM1 and the Plk4-mediated phosphorylation site. The conserved serine residue that is phosphorylated in a Plk4-dependent manner is indicated in red.

E. Total cell extracts were prepared from U2OS cells treated with PCM1 siRNA and transfected with RNAi-resistant EGFP-PCM1-WT*. Cells were cultured asynchronously (As) or arrested in G1, G2 or M phase, followed by immunoprecipitation with an anti-GFP antibodies. Pulled down samples were immunoblotted with the indicated antibodies.

Figure 3. Plk4-mediated phosphorylation of PCM1 at S372 is critical for the proper localisation of centriolar satellites, its dimer formation and interaction with other satellite components

A, B, C, D. siRNA-treated U2OS cells (PCM1 for **A** and **B**; Plk4 for **C** and **D**) were transfected with plasmids producing various EGFP-PCM1 constructs (WT*, S372A*, S372D* or S372E*), fixed and stained with the indicated antibodies (arrowheads point to the centrosome) (**A** and **C**). Quantification data are shown in **B** and **D.** >200 cells were counted and classified into three categories: normal (around and away from the centrosome), aggregated or dispersed. Data represent the mean + SD (n=3). Statistical analysis was performed using two-tailed unpaired student's *t*-tests. ***p<0.001, **p<0.01, *p<0.05, n.s. (not significant). Note that the percentage of cells displaying "dispersed" is analysed. Scale bars, 5 μm (**A** and **C**).

E. PCM1 siRNA-treated U2OS cells were transfected with two types of plasmids (EGFP- and mCherry-tagged) that produce PCM1-WT* and PCM1-S372A*. Immunoprecipitation and subsequent immunoblotting were performed with the indicated antibodies. Quantification data is shown on the right. Statistical analysis was performed using two-tailed unpaired student's *t*-tests. *p<0.05, **p<0.01, n.s. not significant.

F. U2OS cells were treated with PCM1 siRNA and transfected with empty vectors (EV) or EGFP plasmids that produce PCM1-WT* or PCM1-S372A*. Immunoprecipitation was performed with an anti-GFP antibody, followed by immunoblotting with the indicated antibodies.

Figure 4. Plk4-mediated phosphorylation of PCM1 at S372 is essential for ciliogenesis

A. Immunofluorescence microscopy was performed using the indicated antibodies in hTERT-RPE-1 cells treated with control, PCM1 or Plk4 siRNA. Regions around the basal body (insets) are enlarged on the right hand side. Scale bars, 5 μm (left) and 1 μm (right).

B. Quantification. At least 150 cells were counted (n=3). Statistical analysis was performed using two-tailed unpaired student's *t*-tests. ***p<0.001, ****p<0.0001.

C. hTERT-RPE-1 cells treated with PCM1 siRNA were transfected by an empty vector (EV) or plasmids producing PCM1-WT*, -S327A* or -S372E*, and immunofluorescence microscopy performed. Enlarged images of the regions around the basal body are shown in insets. Scale bars, 5 μm and 1 μm (inset).

D. Quantification. At least 200 cells were counted (n=3). Statistical analysis was performed using two-tailed unpaired student's *t*-tests. *p<0.05, **p<0.01, ***p<0.001, ****p<0.0001, n.s. not significant.

E. Model. Plk4 plays a decisive role in not only centriole duplication but also centriolar satellite integrity and primary cilium formation. The latter two roles, at least in part, are executed via PCM1 phosphorylation. Plk4 directly or indirectly phosphorylates PCM1 at S372 (I), which promotes its own dimerisation/oligomerisation (II) and interaction with other components of centriolar satellites (III). These processes ensure PCM1 acts as a structural platform for centriolar satellites. Processes II and III are not necessarily sequential steps. It is shown that centriolar satellites and PCM1 play a critical role in centriole duplication and assembly [25, 49]. Under conditions of serum starvation or developmental cues, centriolar satellites deliver various factors from the cytoplasm to the basal body, thereby helping formation of cilia [26, 30, 37, 50, 51].

Expanded View Figure legends

Figure EV1: Centriolar satellites become dispersed upon depletion of Plk4, but not hSas-6 in both U2OS and HeLa cells

A, B. U2OS cells were transfected with control, Plk4 or hSAS-6 siRNA. 48 h after transfection, cells were fixed and immunostained with antibodies against hMsd1 (**A**, green) or BBS4 (**B**, green) and anti-γ-tubulin antibodies (red). DNA was stained with DAPI (blue). Scale bars, 10 μm.

C. Localisation of the dynein intermediate chain (DIC) is not altered upon Plk4 depletion. U2OS cells were treated with control or Plk4 siRNA and immunostained with antibodies against DIC (red) and Plk4 (green). DNA was stained with DAPI (blue). Scale bar, 5 μm.

D. Efficient depletion of hSAS-6 and Plk4. Protein extracts were prepared from HeLa cells expressing centrin-GFP treated with hSAS-6 (left) or Plk4 siRNA (right). Immunoblotting was performed with the indicated antibodies. The position of protein size markers is shown on the right hand side.

E, F. HeLa cells expressing centrin-GFP were transfected with control, Plk4- or hSAS-6-silencing siRNA, fixed and stained with anti-PCM1 and anti-GFP antibodies or anti-hMsd1/SSX2IP and anti-GFP antibodies. Quantification of cells displaying the dispersed

localisation of PCM1 (**E**) or hMsd1/SSX2IP (**F**) is shown. Data represent the mean + SD (>200 cells, n=3). Statistical analysis was performed using two-tailed unpaired student's *t*-tests. **p<0.01, ****p<0.0001.

G. Experimental scheme of G1 arrest and siRNA treatment. IF, immunofluorescence microscopy; WB, Western blotting (immunoblotting).

H, I. G1 arrested U2OS cells were treated with control or Plk4 siRNA as in **G**. Total cell extracts were prepared and immunoblotting performed with the indicated antibodies (**H**). Band intensities of Plk4 in each sample were quantified using α-tubulin as a loading control (**I**). Statistical analysis was performed using two-tailed unpaired student's *t*-tests. *p<0.05, **p<0.01.

J. Immunoblot showing the protein levels of ectopically expressed Plk4-myc constructs (WT, WT* and kinase dead KD*. * stands for siRNA resistant). U2OS cells were treated with control or Plk4 siRNA, followed by transfection of empty vector plasmids (EV) or those producing various Plk4 versions. Cell extracts were prepared and immunoblotting performed with antibodies against myc and α–tubulin.

K. U2OS cells were treated with control siRNA, and 48 h after transfection, plasmids producing siRNA-resistant Plk4-myc WT* or KD* were further introduced. 24 h after the second transfection, cells were fixed and immunostained with PCM1 (green), myc (blue) and γ-tubulin antibodies (red). Cell peripheries are marked with solid lines, in which cells with yellow lines are successfully transfected (positive in myc signals), while those with white lines represents non-transfected cells. Scale bar, 5 μm.

Figure EV2: Identification of S372 within PCM1 as a phosphorylated residue dependent upon Plk4

A. Plk4-associated PCM1 is phosphorylated. U2OS cells were transfected with Plk4 siRNA, and empty vector plasmids (EV) or those producing siRNA-resistant wild type or kinase dead (KD) myc-Plk4 were introduced.

B. Total cell extracts were prepared from HeLa cells treated with control or Plk4 siRNA, and Immunoprecipitation performed with an anti-PCM1 antibody. Patterns of coomassie brilliant blue (CBB, top) staining and immunoblotting using an anti-PCM1 antibody (bottom) are shown. The position of a protein size marker is shown on the left hand side.

C. Table of identified phosphopeptides. Phosphorylated serines and results of statistical evaluation are shown. Only S372 is hypo-phosphorylated in samples prepared from Plk4 siRNA-treated cells.

D. MS/MS sequence spectrum of S372-phosphorylated QAESLSLTR. -98 denotes loss of H3PO4 and confirms the presence of phosphate. Although the identification is low scoring (MaxQuant score of 52), we have full sequence coverage of the peptide including phosphorylation site position (localisation probability of 0.93).

E. Semi-quantitative analysis of QAESLSLTR containing phosphorylated-S372 performed in Skyline. This phosphopeptide is present in lower abundance in samples prepared from cells treated with Plk4 siRNA.

F. siRNA-treated U2OS cells were transfected with empty vector plasmids (EV) or those producing various EGFP-connected PCM1 proteins (WT*, S372A*, S372D* or S372E*). Immunoblotting was performed by using the indicated antibodies.

G. Validation of the S372 phospho-specific antibody. Samples prepared as in **F** were immunoblotted with S372 phospho-specific and anti-GFP antibodies. Asterisk shows non-specific bands. Phosphorylated bands were only detectable in immunoprecipitates, but not in total extracts (input). Asterisk indicates a non-specific band.

Figure EV3: PCM1-S327A* and PCM1-S327E* result in the dispersion and compromised motility of centriolar satellite, respectively

A, **B**, **C.** PCM1 siRNA treated U2OS cells were transfected with plasmids producing EGFP-PCM1-WT* or -S372A*. Immunofluorescence microscopy was performed with antibodies against γ-tubulin (arrowheads, red), GFP (blue, PCM1) and hMsd1/SSX2IP (green, **A**), BBS4 (green, **B**) or Cep290 (green, **C**). Quantification data is shown on the bottom of each panel. Data represent the mean + SD (>200 cells, n=3). Statistical analysis was performed using two-tailed unpaired student's *t*-tests. *p<0.05, **p<0.01, ***p<0.001. Scale bar, 5 μm.

D, Kymograph analysis of PCM1-WT* and PCM1-S372E* particles. U2OS cells treated with PCM1 siRNA were transfected with plasmids producing EGFP-PCM1-WT* or –S372E*, and time-lapse imaging was performed (n=20 for PCM1-WT*; n=19 for PCM1-S372E*). Scale bar, 1 μm.

E, **F**, **G.** Quantification of PCM1 trajectory shown in **D**. The average velocity (**E**), maximal velocity (**F**) and length (**G**) of PCM1 particles are measured for cells producing PCM1-WT* or PCM1-S372E*. Data represent the mean + SD (>200 cells, n=3). Statistical analysis was performed using two-tailed unpaired student's *t*-tests. ****p<0.0001.

H. U2OS cells were treated with PCM1 siRNA and further transfected with plasmids producing EGFP-PCM1-S372E*. Immunofluorescence microscopy was performed with antibodies against γ-tubulin (red, centrosome marker), GFP (blue) and hMsd1/SSX2IP

(green, top), BBS4 (green, middle) or Cep290 (green, bottom). Enlarged images around the centrosomal region are shown in insets (in which colocalising signals of EGFP-PCM1-S327E* and satellite components are marked by arrowheads). Scale bars, 1 μm (inset), 5 μm.

Figure EV4: Plk4, but not hSAS-6, depletion leads to the dispersion of PCM1 from the centrosomal region in RPE-1 cells

A, B. hTERT-RPE-1 cells were treated with control, PCM1 or Plk4 siRNA. Cell extracts were prepared and immunoblotting was performed with the indicated antibodies. The position of protein size markers is shown on the right hand side.

C. Plk4, but not hSAS-6 depletion leads to the dispersal of PCM1 from the pericentrosomal region. hTERT-RPE-1 cells prepared as in **A** and **B** were immunostained with anti-PCM1 (green) and anti-γ-tubulin antibodies (red). DNA was stained with DAPI (blue). The centrosomes are marked with arrowheads, and cell peripheries are shown with doted lines. Quantification of cells displaying dispersed PCM1 signals is shown on the right. Data represent the mean + SD (>150 cells, n=3). Statistical analysis (right) was performed using two-tailed unpaired student's *t*-tests. *p<0.05, ****p<0.0001. Scale bar, 10 μm.

D. hTERT-RPE-1 cells were transfected with plasmids producing EGFP-PCM1-WT* and asynchronously cultured or serum-starved to induce ciliogenesis for 48 h. Protein extracts were prepared and immunoprecipitation performed with an anti-GFP antibody, followed by immunoblotting with the indicated antibodies.

Expanded View Figure EV1 Hori A. et al

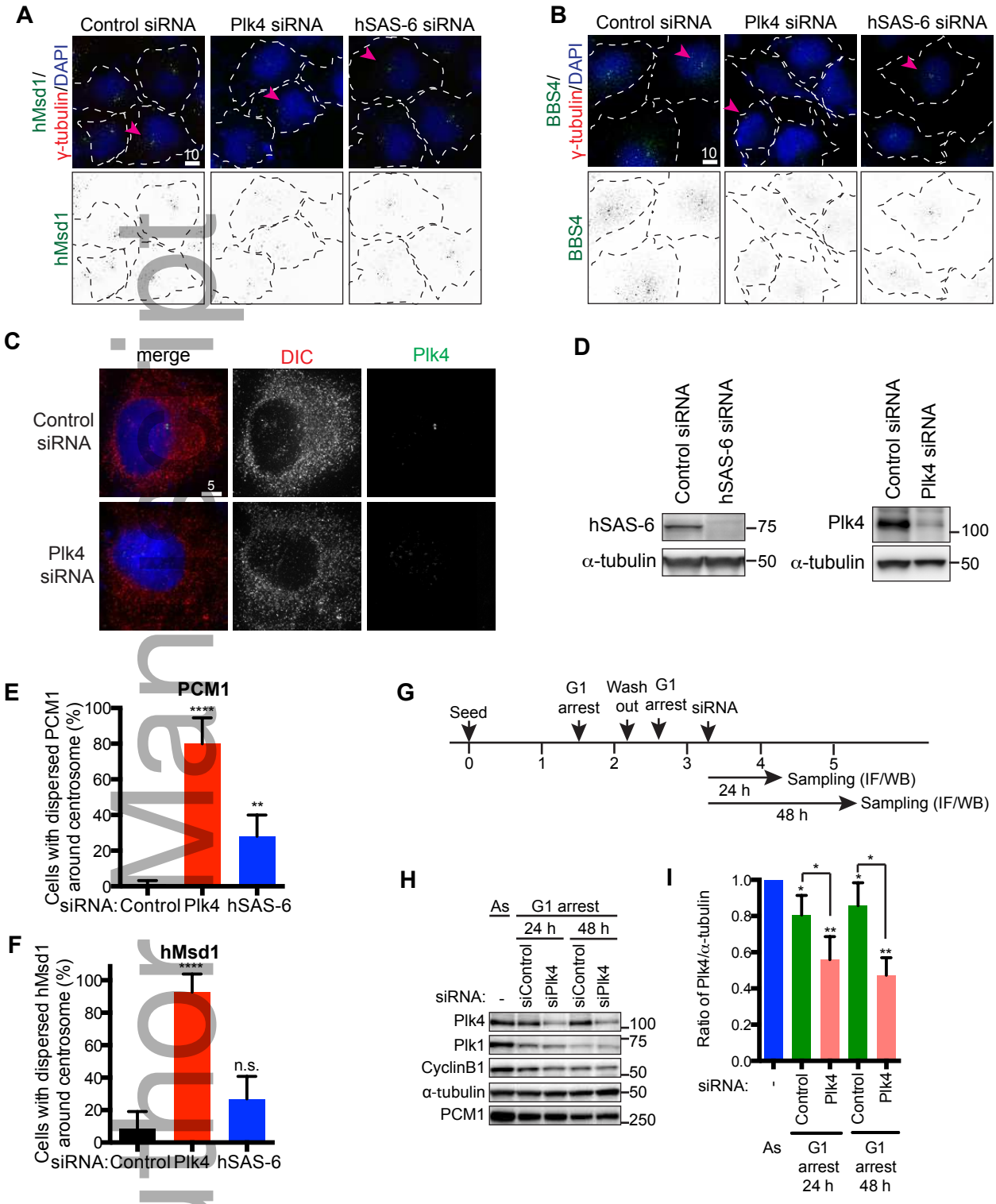

Expanded View Figure EV2 Hori A. et al

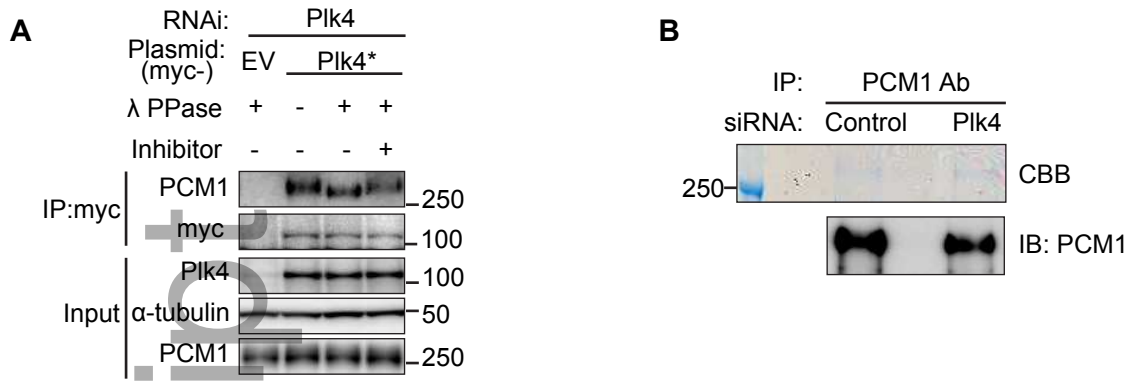

C

Localisation probability	PEP	Score	Position	Modified sequence	Phospho (STY) Probabilities	Number of Phospho (STY)
0.92964	0.0188477	52	372	_QAESLS(ph)LTR_	SQAES(0.032)LS(0.93)LT(0.039)R372	1
0.5	0.0202383	41	643	_S(ph)SLVDEHPEDAEFEQK_	S(0.5)S(0.5)LVDEHPEDAEFEQK	1
0.5	0.0202383	41	644	_S(ph)SLVDEHPEDAEFEQK_	S(0.5)S(0.5)LVDEHPEDAEFEQK	1
0.997945	2.37E-06	78	861	_RQGLAETAS(ph)PVAVSLR_	RQGLAET(0.002)AS(0.998)PVAVSLR	1
	2.37E-06	78	861	_QGLAETAS(ph)PVAVSLR_		1
0.985736	0.00395539	74	1231	_TGFSVS(ph)VEK_	TGFS(0.014)VS(0.986)VEK	1
0.999671	0.00308065	43	1722	_ILEDHGS(ph)PAGEIDDEDKDKDETETVK_	ILEDHGS(1)PAGEIDDEDKDKDETETVK	1

D

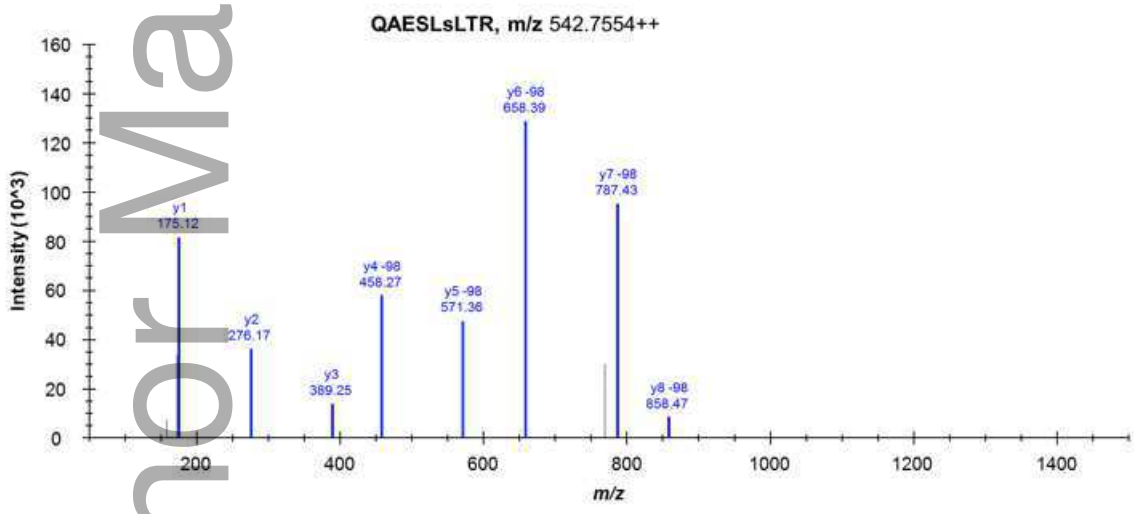

E

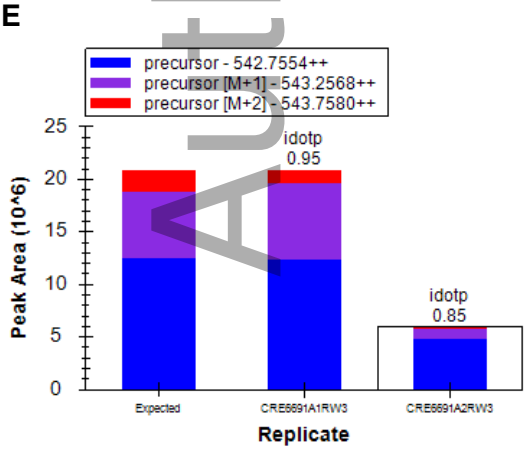

F

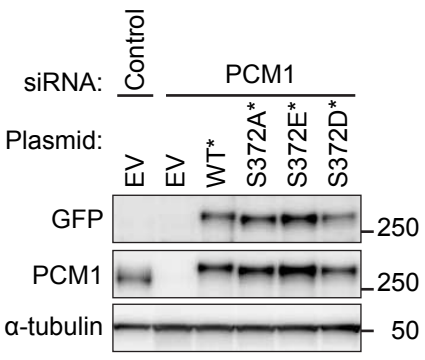

G

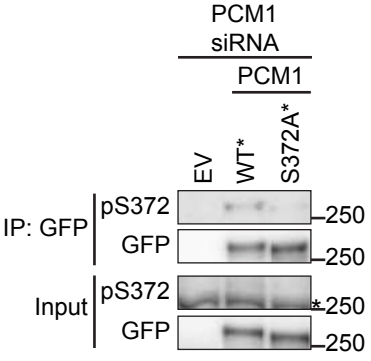

Expanded View Figure EV3 Hori A. et al

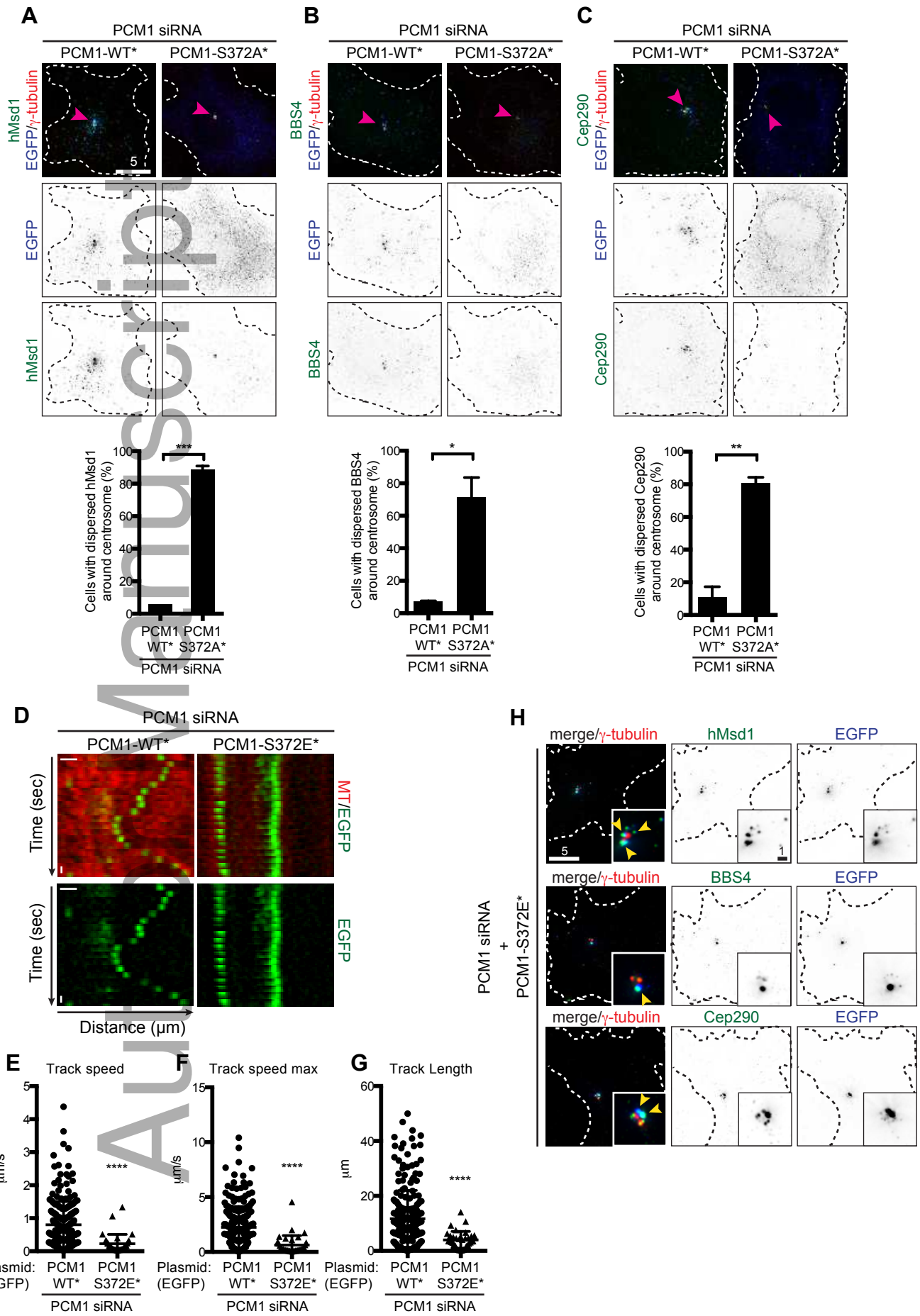

Expanded View Figure EV4 Hori A. et al

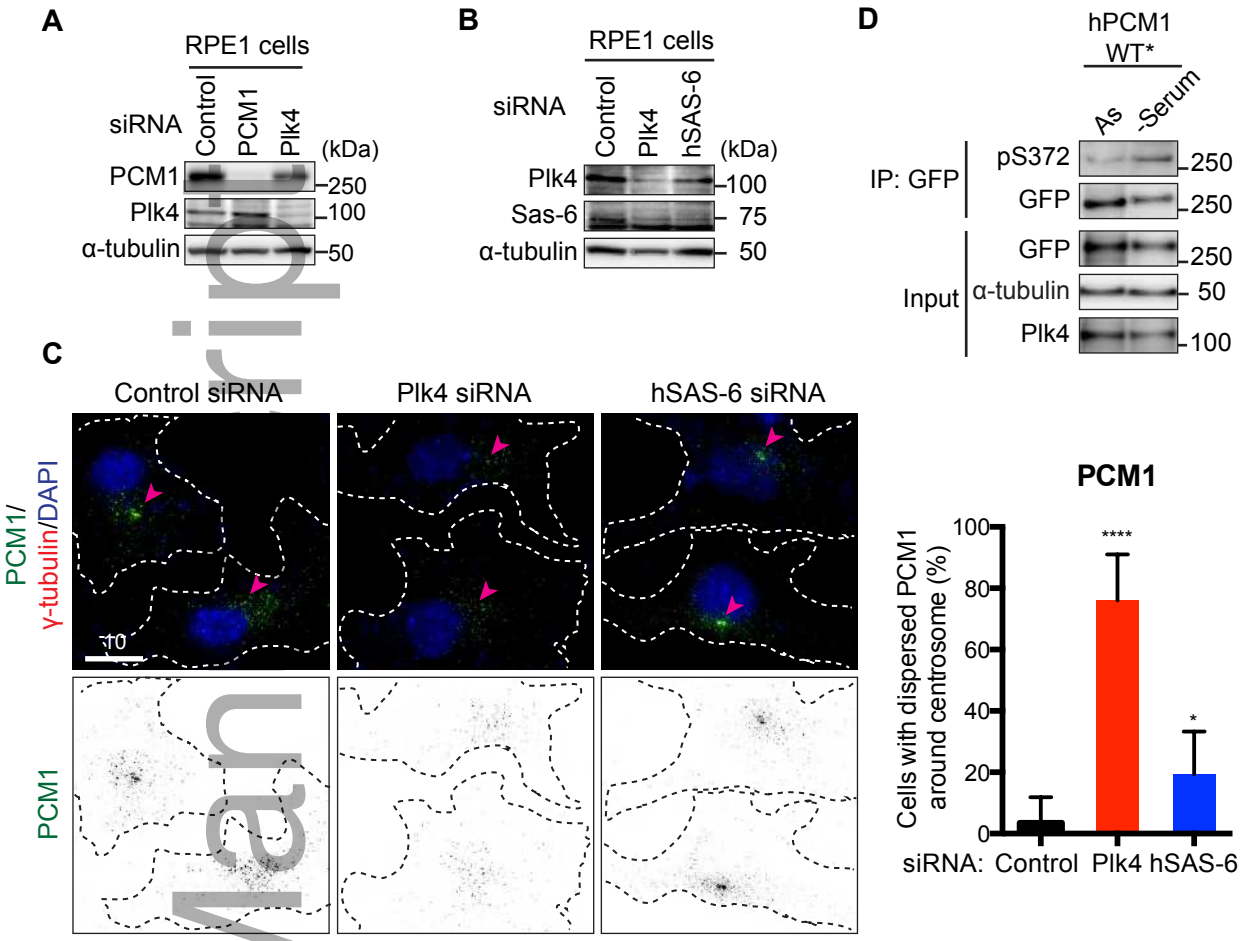

Figure 1 Hori A. et al

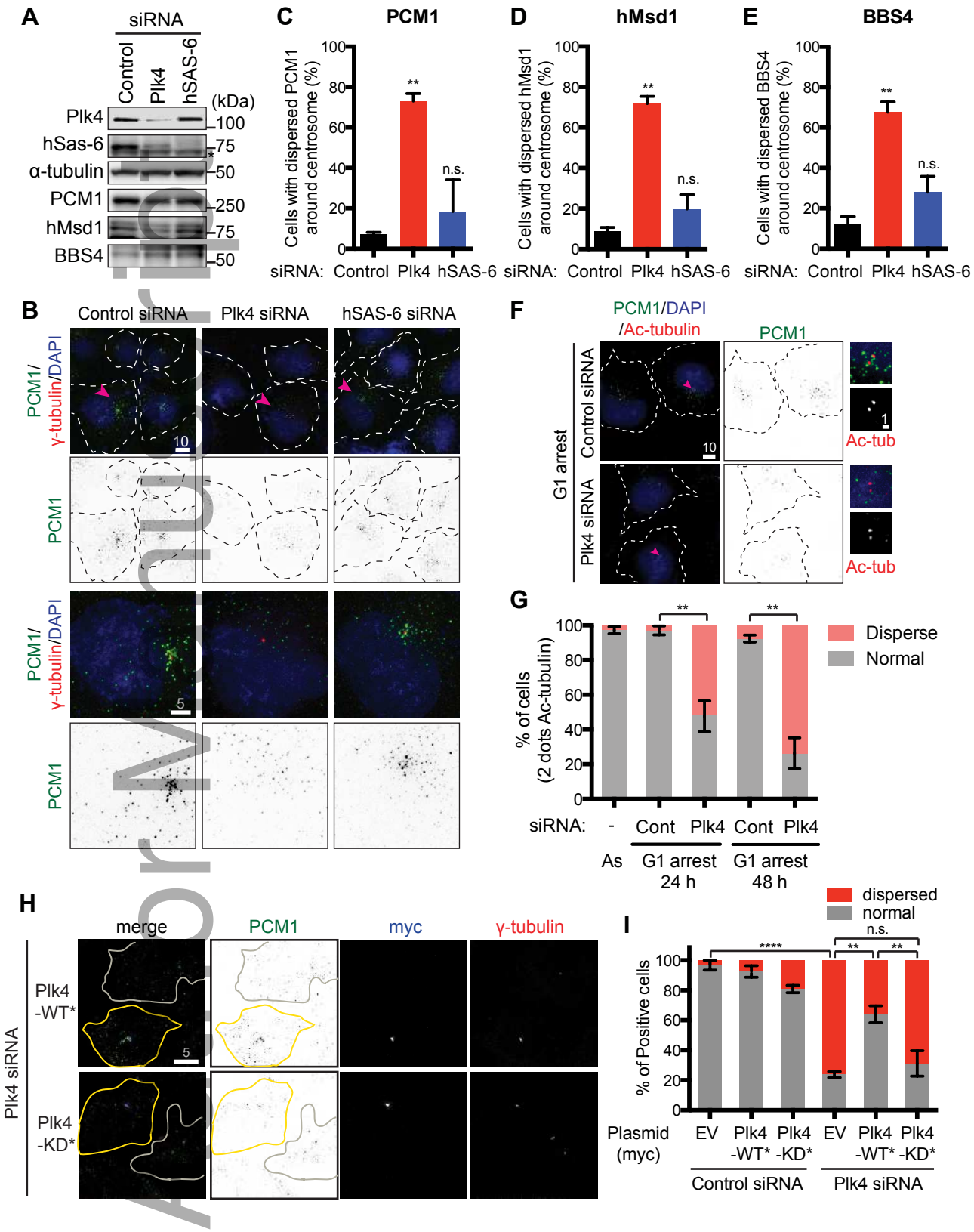

Figure 2 Hori A. et al

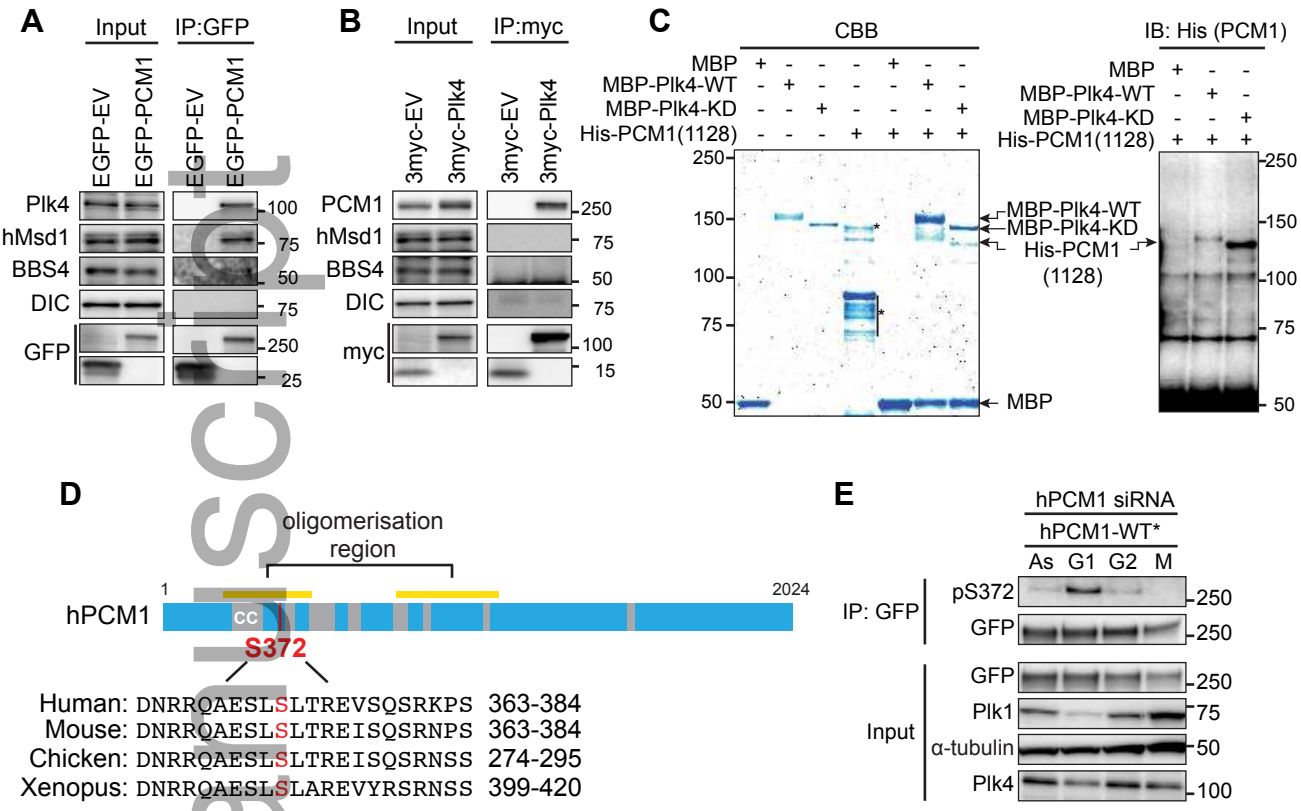

Figure 3 Hori A. et al

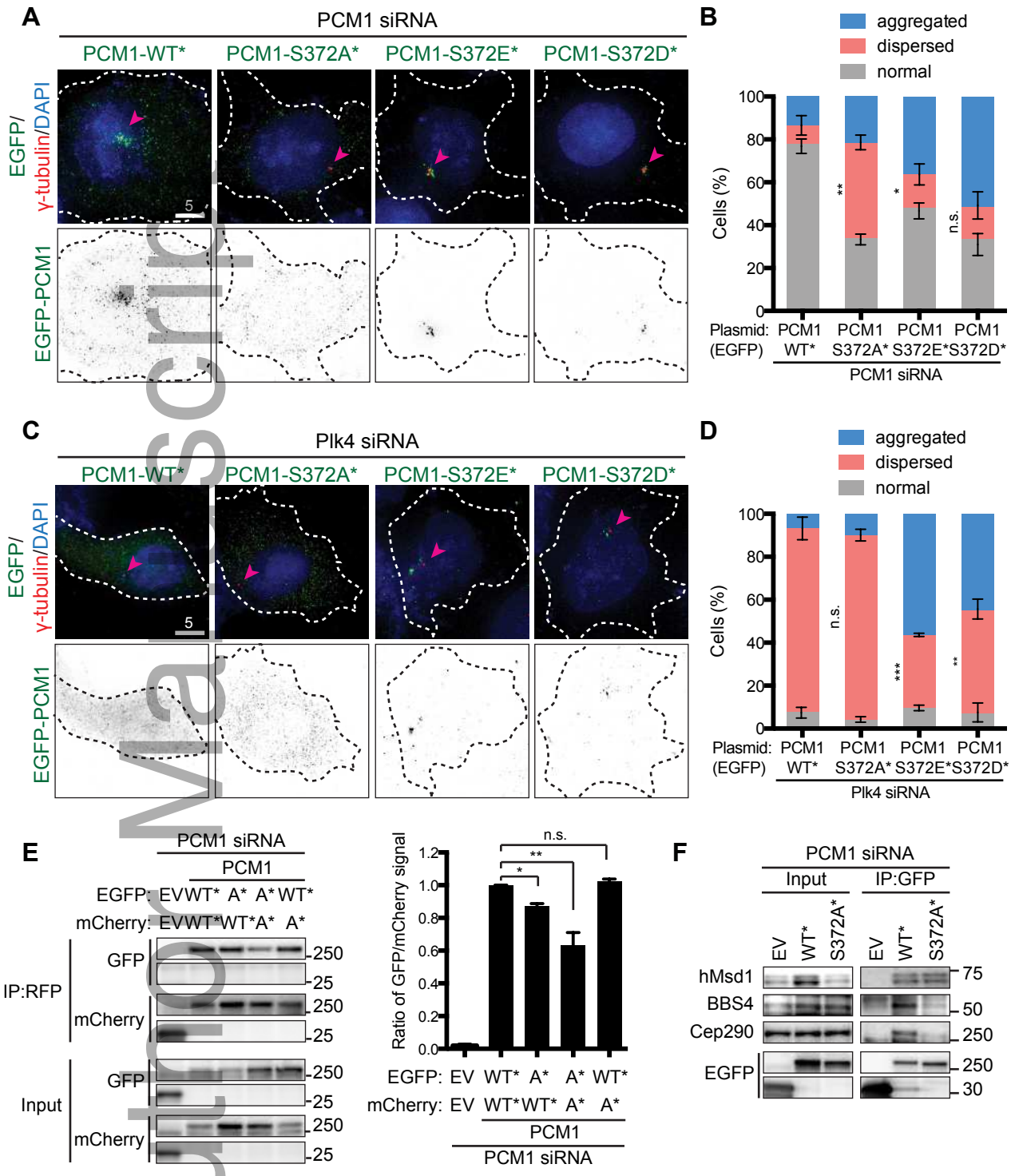

Figure 4 Hori A. et al